

Topological edge states and quantum Hall effect in the Haldane model

Ningning Hao,¹ Ping Zhang,^{2,3,*} Zhigang Wang,² Wei Zhang,² and Yupeng Wang¹

¹*Institute of Physics, Chinese Academy of Sciences, Beijing 100080, People's Republic of China*

²*Institute of Applied Physics and Computational Mathematics,*

P.O. Box 8009, Beijing 100088, People's Republic of China

³*Center for Applied Physics and Technology, Peking University, Beijing 100871, People's Republic of China*

We study the topological edge states of the Haldane's graphene model with zigzag/armchair lattice edges. The Harper equation for solving the energies of the edge states is derived. The results show that there are two edge states in the bulk energy gap, corresponding to the two zero points of the Bloch function on the complex-energy Riemann surface. The edge-state energy loops move around the hole of the Riemann surface in appropriate system parameter regimes. The quantized Hall conductance can be expressed by the winding numbers of the edge states, which reflects the topological feature of the Haldane model.

PACS numbers: 73.43.-f, 73.43.Cd, 71.27.+a

The integer quantum Hall effect (IQHE), discovered in 1980 by Klaus von Klitzing [1], is a striking set of macroscopic quantum phenomena observed in a high mobility two-dimensional electron gas (2DEG) in a strong transverse magnetic field (typically, $B \sim 1\text{--}30\text{T}$). Soon after the Laughlin's famous gauge invariance argument and the treatment of the IQHE as an adiabatic quantum pump [2], it was shortly recognized [3] that the Hall conductance σ_{xy} at the plateaus can be understood in terms of topological invariants known as Chern numbers [4], which are integrals of the k -space Berry curvatures of the bulk states over the magnetic Brillouin zone. While IQHE finds its elegant connection through the adiabatic curvature with bulk topological invariants, Halperin [5] first stressed that the existence of the sample edges, which produces the current-carrying localized edge states in the Landau energy gap, is essential in the Laughlin's gauge invariance argument. Hatsugai further developed a topological theory of the edge states [6], in which topological invariants are the winding numbers of the edge states on the complex-energy Riemann surface (RS).

The presence of IQHE fundamentally rely on the breaking of the time-reversal symmetry (TRS), which in the above mentioned works is brought about by imposing an external magnetic field on the electrons. Besides this external magnetic field, the TRS also can be broken by a variety of the other extrinsic or intrinsic mechanisms. A most straightforward way is, like what has been carried out in the Aharonov-Bohm (AB) effect, the introduction of magnetic flux (instead of magnetic field) to the Bloch electrons. In virtue of such a way, by using a graphene lattice with the complex hopping matrix elements of the next-nearest-neighboring honeycomb sites included, Haldane first showed that the non-zero Chern numbers and thus the IQHE can be realized in zero magnetic field [7]. In contrast with the cases with external magnetic field, a detailed study of the topological edge states of the Hal-

dane model is still lacking. This issue is stressed in the present paper. Also, our study is motivated by the observation that in addition to its importance in charge IQHE, the spin-doubled Haldane model, in which TRS is recovered, has also played a key role in understanding the quantum spin Hall effect (QSHE) [10] and new phase of matter [11].

Our discussion of the topological edge states for the Haldane model begins with deriving the Harper equation to describe the wave-function transfer relation between two edges in a graphene ribbon. It is found that there are two edge states in the bulk energy gap, corresponding to two zero points of the Bloch function on the complex-energy RS. The edge-state energy loops move around the hole of the RS, giving rise to nontrivial winding numbers. The quantized Hall conductance can be expressed by the winding numbers of the edge states, which reflects the topological feature of the Haldane model.

The graphene lattice is composed of two sublattices (denoted by the red and blue dots in Fig. 1). The graphene ribbons with zigzag edges and armchair edges are plotted in Fig. 1(a) and 1(b), respectively. The lattice tight-binding Hamiltonian [7] is given by

$$H = \sum_i t_0 c_i^\dagger c_i + \sum_{\langle i,j \rangle} t_1 c_i^\dagger c_j + \sum_{\langle\langle i,j \rangle\rangle} t_2 e^{i\phi_{ij}} c_i^\dagger c_j. \quad (1)$$

In the above Hamiltonian, the on-site energy $t_0 = +M$ on A site and $-M$ on B site. t_1 and t_2 are real hopping matrix elements between nearest neighbors on the different and the same sublattices, respectively. To break TRS, a complex phase ϕ_{ij} is introduced to the next nearest neighbor hopping t_2 . Following Haldane [7], we set the magnitude of this complex phase as $|\phi_{ij}| = \phi$, and the direction of the positive phase is anticlockwise. Note that the net flux is zero in one unit cell. Since the spin-orbital effect is not included, we neglect the spin indices for simplicity.

Now, let us derive the Harper equation [8, 9] of the graphene ribbons with zigzag edges. We suppose that the system is periodic in the x direction while it has two

*E-mail: zhang_ping@iapcm.ac.cn

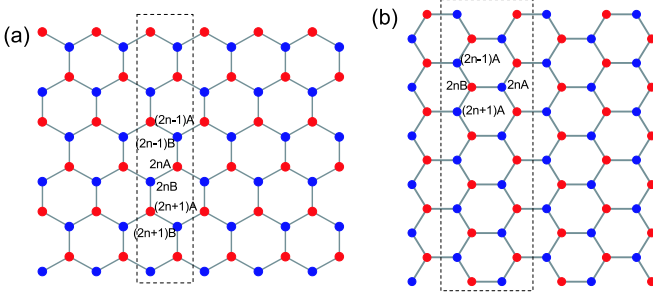


FIG. 1: (Color online) The structure of graphene ribbons with (a) zigzag edges and (b) armchair edges. The rectangle with the dashed line is the unit cell.

edges in the y direction [see Fig. 1(a)]. In the following we replace index i with (mns) to denote the lattice site, where (mn) label the unit cells and s label the sites A and B in this cell. The distance of the nearest neighboring lattice sites is set to be unity throughout this paper. Since the lattice is periodic in the x direction, we can use a momentum representation of the electron operator

$$c_{mns} = \frac{1}{\sqrt{L_x}} \sum_{k_x} e^{ik_x X_{mns}} c_{ns}(k_x), \quad (2)$$

where (X_{mns}, Y_{mns}) represents the coordinate of the site s in the unit cell (mn) , and k_x is the momentum along the x direction. Let us consider the one-particle state $|\psi(k_x)\rangle = \sum \psi_{ns}(k_x) c_{ns}^\dagger(k_x) |0\rangle$. Inserting it into the Schrödinger equation $H|\psi\rangle = \epsilon|\psi\rangle$, one can easily get the following two eigenvalue equations for sites A and B:

$$\begin{aligned} \epsilon\psi_{nA} &= (M + f_+) \psi_{nA} + g_- (\psi_{(n+1)A} + \psi_{(n-1)A}) \\ &\quad + t_1 \psi_{(n-1)B} + g_0 \psi_{nB}, \\ \epsilon\psi_{nB} &= (-M + f_-) \psi_{nB} + g_+ (\psi_{(n+1)B} + \psi_{(n-1)B}) \\ &\quad + t_1 \psi_{(n+1)A} + g_0 \psi_{nA}, \end{aligned} \quad (3)$$

where $f_{\pm} = 2t_2 \cos(\sqrt{3}k_x \pm \phi)$, $g_{\pm} = 2t_2 \cos(\frac{\sqrt{3}}{2}k_x \pm \phi)$, and $g_0 = 2t_1 \cos(\frac{\sqrt{3}}{2}k_x)$. Eliminating the B sites, we obtain a difference equation for A sites

$$\psi_n = b(\psi_{(n-1)} + \psi_{(n-3)}) + d\psi_{(n-2)} - \psi_{(n-4)}, \quad (4)$$

where

$$\begin{aligned} b &= \frac{1}{g_+ g_-} \left\{ 2(g_+ + g_-)\epsilon + 2g_0 \left[t_1 - \frac{t_2^2}{t_1} \right] \right. \\ &\quad \left. + \frac{t_2}{t_1} g_0 M \sin \phi - 4t_2^2 \cos\left(\frac{3\sqrt{3}}{2}k_x\right) \cos 2\phi \right\}, \\ d &= \frac{1}{g_+ g_-} \left\{ 2(M^2 + t_1^2 - \epsilon^2) - f_+ f_- \right. \\ &\quad \left. + 4t_2 \left[\frac{g_0^2}{t_1^2} - 2 \right] (\epsilon \cos \phi - M \sin \phi) \right\} - 2, \end{aligned} \quad (5)$$

and ψ_{nA} was replaced by ψ_n . Eq. (4) is the so-called Harper equation [8, 9]. The next key step is to represent Eq. (4) in the transfer matrix form. After a tedious but straightforward derivation, we find that by introduction of a new wave function φ_n , which is a linear transformation of the original wave function ψ_n ,

$$\varphi_n = \psi_n + \frac{-b + \sqrt{b^2 + 4(2+d)}}{2} \psi_{n-1} + \psi_{n-2}, \quad (6)$$

then the new wave function φ_n can be written in the following transfer matrix form

$$\begin{pmatrix} \varphi_n \\ \varphi_{n-1} \end{pmatrix} = \begin{pmatrix} t & -1 \\ 1 & 0 \end{pmatrix} \begin{pmatrix} \varphi_{n-1} \\ \varphi_{n-2} \end{pmatrix} \equiv \widetilde{M}(\epsilon) \begin{pmatrix} \varphi_{n-1} \\ \varphi_{n-2} \end{pmatrix}, \quad (7)$$

where $t = \frac{b + \sqrt{b^2 + 4(2+d)}}{2}$. More generally, we take φ_0 and φ_{L_y} as the wave functions at two open edges. Then we get a reduced transfer matrix linking the two edges as follows:

$$\begin{pmatrix} \varphi_{L_y+1} \\ \varphi_{L_y} \end{pmatrix} = M(\epsilon) \begin{pmatrix} \varphi_1 \\ \varphi_0 \end{pmatrix}, \quad (8)$$

where

$$M(\epsilon) = [\widetilde{M}(\epsilon)]^{L_y} = \begin{pmatrix} M_{11}(\epsilon) & M_{12}(\epsilon) \\ M_{21}(\epsilon) & M_{22}(\epsilon) \end{pmatrix}. \quad (9)$$

All kind of solutions of Eq. (8) are obtained by different choices of φ_0 and φ_1 .

Similarly, one can obtain the eigenvalue equations of a graphene ribbon with armchair edges,

$$\begin{aligned} (\epsilon - M)\psi_{nA} &= t_1 e^{-ika} \psi_{nB} + t_1 e^{i\frac{ka}{2}} [\psi_{(n+1)B} + \psi_{(n-1)B}] \\ &\quad + t_2 [e^{-i\phi} \psi_{(n+2)A} + e^{i\phi} \psi_{(n-2)A}] \\ &\quad + \frac{t_2}{t_1} g_0 [e^{i\phi} \psi_{(n+1)A} + e^{-i\phi} \psi_{(n-1)A}], \\ (\epsilon + M)\psi_{nB} &= t_1 e^{ika} \psi_{nA} + t_1 e^{-i\frac{ka}{2}} [\psi_{(n+1)A} + \psi_{(n-1)A}] \\ &\quad + t_2 [e^{i\phi} \psi_{(n+2)B} + e^{-i\phi} \psi_{(n-2)B}] \\ &\quad + \frac{t_2}{t_1} g_0 [e^{-i\phi} \psi_{(n+1)B} + e^{i\phi} \psi_{(n-1)B}]. \end{aligned} \quad (10)$$

However, because the derivation of the Harper equation for a graphene ribbon with armchair edges is too sophisticated, here we do not write out the transfer-matrix expression of this Harper equation. Moreover, because the main results and the discussions on the graphene ribbons with zigzag and armchair edges are similar, in the following we focus our attention to the graphene with zigzag edges. The general open boundary condition is

$$\varphi_{L_y} = \varphi_0 = 0. \quad (11)$$

With Eqs. (8) and (9), one can easily get that the solutions satisfy

$$M_{21}(\epsilon) = 0 \quad (12)$$

and

$$\varphi_{L_y-1} = -M_{11}(\epsilon) \varphi_1. \quad (13)$$

If we use a usual normalized wave function, the state is localized at the edges as

$$\begin{cases} |M_{11}(\epsilon)| \ll 1 \text{ localized at } y \approx 1 \text{ (down edge),} \\ |M_{11}(\epsilon)| \gg 1 \text{ localized at } y \approx L_y - 1 \text{ (up edge).} \end{cases} \quad (14)$$

Because the analytical derivation of the energy spectrum in the presence of edges is very difficult, we now start a numerical calculation from Eqs. (3) and (10). Varying all the controllable parameters, which are the relative site energy M/t_1 , the next nearest neighbor hopping t_2/t_1 , and the complex phase ϕ , we can get three different cases happening in the energy spectrum of the graphene ribbons. We draw in Figs. 2(a)-(c) [Figs. 3(a)-(c)] the energy spectrum of graphene ribbons with zigzag (armchair) edges as a function of k_x for these three different cases, i.e., the case $M/t_2 < 3\sqrt{3}\sin\phi$ (case I), the case $M/t_2 < -3\sqrt{3}\sin\phi$ (case II), and the case $M/t_2 > 3\sqrt{3}|\sin\phi|$ (case III), respectively. The number of sites A (B) in y direction is chosen to be $L_y=40$. Clearly, from Figs. 2 and 3 one can see that there are two dispersed energy bands (the shaded areas) with two edge states (the colored lines) lying in the energy gap. It is our task to show that the geometric nature of the edge states in these three kinds of parameter regions are totally different, which can be described by the winding numbers of the edge states on a complex energy RS within the topological edge theory [6].

To show this, first, we ignore the open boundary condition and consider the bulk Bloch function at sites with y -coordinate of (L_y-1) . For Bloch function, $\varphi_0^{(b)}$ and $\varphi_1^{(b)}$ compose an eigenvector of M with the eigenvalue ρ ,

$$M(\epsilon) \begin{pmatrix} \varphi_1^{(b)} \\ \varphi_0^{(b)} \end{pmatrix} = \rho(\epsilon) \begin{pmatrix} \varphi_1^{(b)} \\ \varphi_0^{(b)} \end{pmatrix}. \quad (15)$$

In order to discuss the wave function of the edge state, we extend the energy to a complex energy. In the following, we use a complex variable z instead of real energy ϵ . From Eq. (15) we get

$$\rho(z) = \frac{1}{2} \left[\Delta(z) - \sqrt{\Delta^2(z) - 4} \right] \quad (16)$$

and

$$\varphi_{L_y-1} = -\frac{M_{11}(z) + M_{22}(z) - \omega}{-M_{11}(z) + M_{22}(z) + \omega} M_{21}(z) \varphi_1, \quad (17)$$

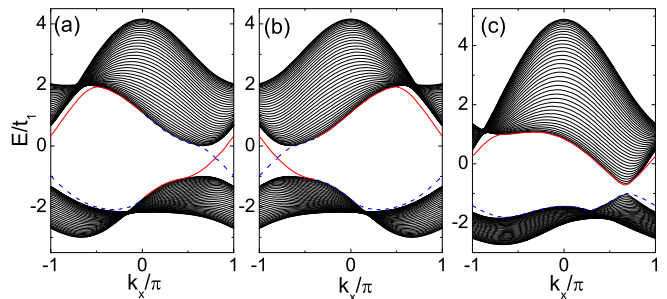


FIG. 2: (Color online) Energy spectrum of the graphene ribbon with zigzag edges under different complex phases parameters: (a) $\phi=\pi/3$, (b) $\phi=-\pi/3$, (c) $\phi=\pi/6$. The other parameters are set as $M/t_1=1$ and $t_2/t_1=1/3$ in all three figures. The shaded areas are the energy bands and the colored lines are the spectrum of the edge states. The red (solid) and blue (dashed) lines mean that the edge states are localized near the down and up edges, respectively.

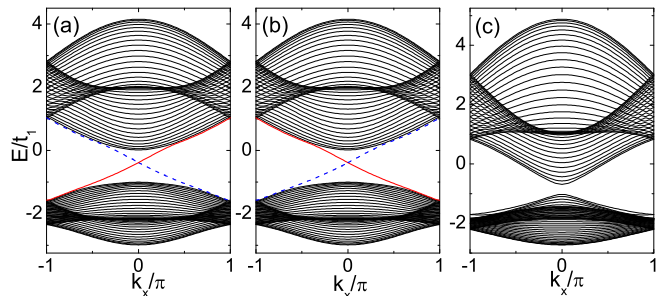


FIG. 3: (Color online) Energy spectrum of the graphene ribbon with armchair edges under different complex phases parameters: (a) $\phi=\pi/3$, (b) $\phi=-\pi/3$, (c) $\phi=\pi/6$. The other parameters are set as $M/t_1=1$ and $t_2/t_1=1/3$ in all three figures. The shaded areas are the energy bands and the colored lines are the spectrum of the edge states. The red (solid) and blue (dashed) lines mean that the edge states are localized near the down and up edges, respectively.

where $\Delta(z)=\text{Tr}[M(z)]$ and $\omega=\sqrt{\Delta^2(z)-4}$. Clearly,

$$\det M(\epsilon) = 1 \quad (18)$$

since $\det \widetilde{M}(\epsilon)=1$. From Eq. (17) one can find that the analytic structure of the wave function is determined by the algebraic function $\omega=\sqrt{\Delta^2(z)-4}$. The RS of $\omega=\sqrt{\Delta^2(z)-4}$ on the complex energy plane can be built by the conglutination between different analytic brunches. Here, the close complex energy plane can be obtained from the open complex energy plane through spherical pole mapping [see Fig. 4(a)]. Now let us discuss the analytic structure of $\omega = \sqrt{\Delta^2(z)-4}$ on the open complex energy plane. If the system has q energy bands, i.e.,

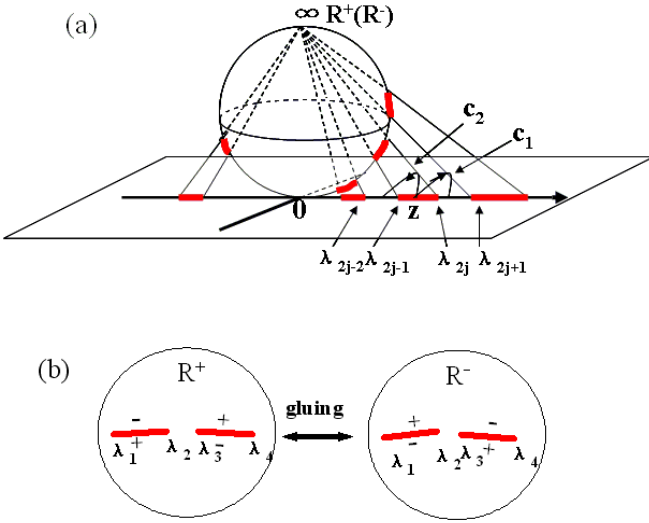


FIG. 4: (Color online) (a) The open complex energy plane are mapped to the close complex energy plane through spherical pole projection. (b) Two sheets with two cuts which correspond to the energy bands of the graphene nanoribbons. The RS of the Bloch function is obtained by gluing the two spheres along the arrows near the cuts.

$$\epsilon \in [\lambda_1, \lambda_2], \dots, [\lambda_{2j-1}, \lambda_{2j}], \dots, [\lambda_{2q-1}, \lambda_{2q}], \quad (19)$$

where λ_j denote energies of the band edges and $\lambda_i < \lambda_j$, $i < j$, then ω can be factorized as

$$\omega = \sqrt{\Delta^2(z) - 4} = \sqrt{\prod_{j=1}^{2q} (z - \lambda_j)}. \quad (20)$$

In the present Haldane model, there are two energy bands, so $q=2$. The two single-value analytic branches are defined on the same complex energy plane with q secants. The difference between the two branches are specified in the following paragraph.

For an up- or down-edge-state energy μ_j in the gap $[\lambda_{2j}, \lambda_{2j+1}]$, In order to ensure $\omega(\mu_j) \geq 0$, we divide the two single-value analytic branches in terms of the parity (evenness or oddness) of j . Let us consider the case that the energy z lies in the band $[\lambda_{2j-1}, \lambda_{2j}]$ [see Fig. 4(a)]. The left side of this energy band is the $(j-1)$ th gap, while the right side is the j th gap. When the energy z moves from the j th band to the $(j-1)$ th gap (the j th gap) along an arbitrary path c_1 (c_2), only the singularities λ_{2j-1} and λ_{2j} have contributions to the variance of the principal value of the argument of ω . On the up bank of the secant, we distinguish two branches R^+ and R^- as the following: For even values of j , if we set $\arg(z - \lambda_{2j-1})=0$ and $\arg(z - \lambda_{2j})=\pi$, which corresponds to $\omega(\mu_{j-1}) > 0$ ($\omega(\mu_j) < 0$) when z moves along c_1 (c_2), then the branch R^+ is defined as a complex plane

with q secants. Whereas, if we set $\arg(z - \lambda_{2j-1})=2\pi$ and $\arg(z - \lambda_{2j})=\pi$, which corresponds to $\omega(\mu_{j-1}) < 0$ ($\omega(\mu_j) > 0$) when z moves along c_1 (c_2), then the branch R^- is defined as a complex plane with q secants. The definitions of R^+ and R^- for odd values of j are reverse to those for even values of j . So, if z lies in the j th gap from below on the real axis,

$$\alpha(-1)^j \omega \geq 0, \quad z: \text{real on } R^\alpha \quad (\alpha = +, -),$$

and at energies $\mu_j (\in R^\alpha, \alpha = +, -)$ of the edge states we have

$$\omega(\mu_j) = \alpha(-1)^j |M_{11}(\mu_j) - M_{22}(\mu_j)|, \quad (21)$$

In addition, one can easily obtain

$$\Delta(\epsilon) \begin{cases} \leq -2 & \text{for } j \text{ odd} \\ \geq 2 & \text{for } j \text{ even} \end{cases}, \quad (22)$$

where the energy ϵ (on R^α) is in the j th gap.

When the branches R^+ and R^- on the open complex energy plane are mapped to the close complex energy plane through spherical-pole-projection, one can get two single-value analytic spherical surfaces. The RS is obtained by gluing the two spherical surfaces at these branch cuts with making sure that the \pm banks face the \mp banks of other sphere [see Figs. 4(b)]. Note that there are two real axes after gluing. In the present model the genus of the RS is $g=1$, which is the number of energy gaps. The wave function is defined on the $g=1$ RS $\Sigma_{g=1}(k_x)$. The branch of the Bloch function is specified as $\omega > 0$, which we have discussed above. With Eqs. (22), (21) and (17), and using the fact that $\varphi_{L_{y-1}}(\mu_j)=0$ for $\mu_j \in R^\alpha$ and $\varphi_{L_{y-1}}(\mu_j) \neq 0$ for $\mu_j \in R^{-\alpha}$, one can obtain that when the zero point is on the upper sheet of RS (R^+), the edge state is localized at the down edge; when the zero point is on the lower sheet of RS (R^-), the edge state is localized at the up edge.

Figure 5(a)-(c) schematically show the RS's for the present Haldane model with the system parameters belonging to case-I ($M/t_2 < 3\sqrt{3}\sin\phi$), case-II ($M/t_2 < -3\sqrt{3}\sin\phi$), and case-III ($M/t_2 > 3\sqrt{3}|\sin\phi|$), respectively. On each RS $\Sigma_{g=1}(k_x)$ the energy gap corresponds to the loop around the hole of the $\Sigma_{g=1}(k_x)$ and the energy bands correspond to the closed paths vertical to the energy gap loop on $\Sigma_{g=1}(k_x)$. The Bloch function is defined on this surface. For the fixed k_x and ϕ , there is always $g=1$ zero point at the down-edge-state energy $\mu_j^{(\text{down})}$. Since there are two real axes on the $\Sigma_{g=1}(k_x)$, correspondingly, there is $g=1$ zero point at the up-edge-state energy $\mu_j^{(\text{up})}$.

The above analysis is for the fixed k_x . Changing k_x in one period, we can consider a family of RS's $\Sigma_{g=1}(k_x)$. $\Sigma_{g=1}(k_x)$ can be modified by this change. However, all the RS's $\Sigma_{g=1}(k_x)$ with different k_x are topologically

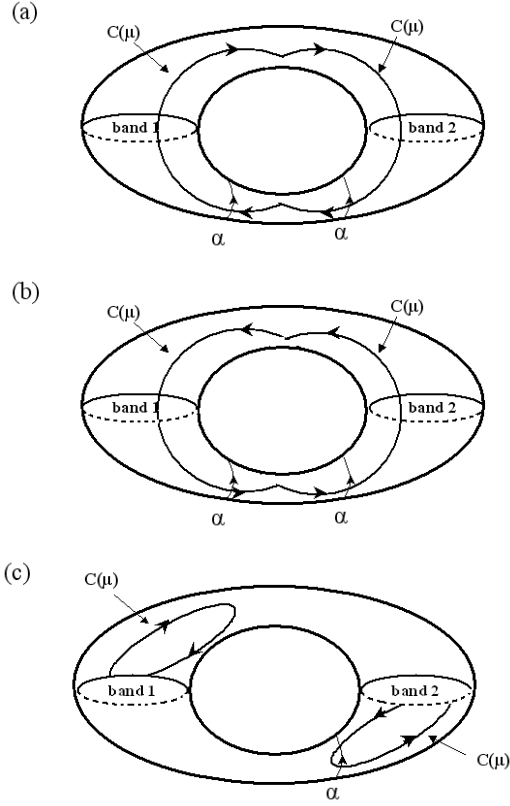


FIG. 5: Riemann surfaces of the Bloch functions for different winding numbers: (a) $I=1$, (b) $I=-1$, and (c) $I=0$.

equivalent if, as what happens in the present model, there are stable energy gaps in the 2D energy spectrum. By identifying the topologically equivalent RS's $\Sigma_{g=1}(k_x)$, the behavior of the track of $\mu_j(k_x)$ (including the up-edge-state energy $\mu_j^{(\text{up})}$ and down-edge-state energy $\mu_j^{(\text{down})}$) depends on system parameters, as shown in Fig. 5. In Fig. 5(a), which corresponds to case-I of $M/t_2 < 3\sqrt{3}\sin\phi$, one can observe that by varying k_x , the down-edge-state energy $\mu_j^{(\text{down})}(k_x)$ moves from the lower band (band 1 in Fig. 5) edge to the upper band (band 2 in Fig. 5) edge, while the down-edge-state energy $\mu_j^{(\text{down})}(k_x)$ moves from the upper band edge to the lower band edge. That is to say, the two edge-state energy tracks in the same energy gap move around the hole and form an oriented loop $C(\mu_j)$. In case-II of $M/t_2 < -3\sqrt{3}\sin\phi$, as shown in Fig. 5(b), the two edge-state energy tracks moving around the hole also form an oriented loop. However, the orientation of the loop is right about with respect to that in case-I. Finally, in case-III of $M/t_2 > 3\sqrt{3}|\sin\phi|$, as shown in Fig. 5(c), one can observe that the $\mu_j(k_x)$ moves along the hole and turns back before arriving at the second energy band. In this case, the two edge-state energy tracks in the same energy gap approximately form two circularities.

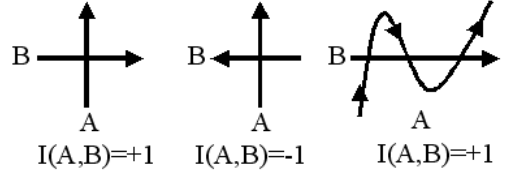


FIG. 6: Intersection number $I(A, B)$ of two curves A and B. Each intersection point contributes by +1 or -1 according to the direction.

It is known that on a general genus- g RS, all kinds of loops (the first homotopy group) are generated by $2g$ canonical loops (generators), α_i and β_i , $i=1, \dots, g$. See Fig. 5 for $g=1$. The intersection number of these curves (including directions) [6] is given by (see Fig. 6)

$$I(\alpha_i, \beta_j) = \delta_{ij}. \quad (23)$$

Any curves on the RS are spanned homotopically by α_i and β_i . When the edge-state energy loop $\mu_j(k_x)$ moves p times around the j th hole with some integer p , one has

$$C(\mu_j) \approx \beta_j^p, \quad (24)$$

which means

$$I(\alpha_i, C(\mu_j)) = p\delta_{ij}. \quad (25)$$

When the Fermi energy ϵ_F of the 2D system lies in the j th bulk energy gap, the Hall conductance is given by the winding number of the edge state [6], which is given by the number of intersections $I(\alpha_j, C(\mu_j))$ ($\equiv I(C(\mu_j))$) between the canonical loop α_j on the RS and the trace of μ_j . In the present single-gap model, we obtain the Hall conductance provided by the edge states as follows

$$\sigma_{xy}^{\text{edge}} = -\frac{e^2}{h} I(C(\mu)). \quad (26)$$

From Figs. 5(a) and (b) it can be observed that μ moves one time across the hole ($p=1$), which in terms of Eq. (24) means $C(\mu) \approx \beta$. Considering simultaneously the winding direction (see Fig. 6), one can obtain that in Fig. 5(a) $I(C(\mu))=-1$, while in Fig. 5(b) $I(C(\mu))=1$. In Fig. 5(c), because $p=0$, $I(\alpha_i, C(\mu_i))=0$ and the Hall conductivity is zero. Therefore, we get

$$\sigma_{xy}^{\text{edge}} = \begin{cases} \frac{e^2}{h}, & M/t_2 < 3\sqrt{3}\sin\phi \\ 0, & M/t_2 > 3\sqrt{3}|\sin\phi| \\ -\frac{e^2}{h}, & M/t_2 < -3\sqrt{3}\sin\phi \end{cases}. \quad (28)$$

Finally, let us compare this result for the graphene ribbons with zigzag/armchair edges with the bulk graphene,

in which the topological invariant is the Chern number. In the bulk Haldane model, when the Fermi energy ϵ_F lies in the energy gap, the Hall conductance is quantized as $\sigma_{xy}^{\text{bulk}} = \frac{e^2}{h} C_1$, where C_1 is the Chern number of the lower energy band. It turns out that

$$C_1 = \begin{cases} 1, & M/t_2 < 3\sqrt{3}\sin\phi \\ 0, & M/t_2 > 3\sqrt{3}|\sin\phi| \\ -1, & M/t_2 < -3\sqrt{3}\sin\phi \end{cases}. \quad (29)$$

From Eqs. (28) and (29) one can obtain $\sigma_{xy}^{\text{edge}} = \sigma_{xy}^{\text{bulk}}$, which is in accord with the established recognition [5, 6] on the Hall conductance in the systems with and without

edges.

In summary, we have investigated the topological property of the edge states in the Haldane model. The Harper equations for solving and analyzing the edge states have been derived. It has been found that there are two edge states lying in the bulk energy gap. These two edge states move with varying k_x around the hole in the RS and form an orientated energy loop. With the winding number of the edge states, we have obtained that the edge-state Hall conductance is $\sigma_{xy}^{\text{edge}} = \pm \frac{e^2}{h}$ or 0 under different cases, which agrees with that based on the topological bulk theory.

-
- [1] K. von Klitzing, G. Dorda, and M. Pepper, Phys. Rev. Lett. **45**, 494 (1980).
[2] R. B. Laughlin, Phys. Rev. B **23**, 5632 (1981).
[3] D. Thouless, M. Kohmoto, M. Nightingale, and M. den Nijs, Phys. Rev. Lett. **49**, 405 (1982).
[4] D. J. Thouless, *Topological Quantum Numbers in Nonrelativistic Physics* (World Scientific, Singapore, 1998).
[5] B. I. Halperin, Phys. Rev. B **25**, 2185 (1982).
[6] Y. Hatsugai, Phys. Rev. Lett. **71**, 3697 (1993); Phys. Rev. B **48**, 11851 (1993).
[7] F. D. M. Haldane, Phys. Rev. Lett. **61**, 2015 (1988).
[8] P. G. Harper, Proc. Phys. Soc. London Sect. A **68**, 874 (1955).
[9] D. R. Hofstadter, Phys. Rev. B **14**, 2239 (1976).
[10] C. L. Kane and E. J. Mele, Phys. Rev. Lett. **95**, 226801 (2005).
[11] C. L. Kane and E. J. Mele, Phys. Rev. Lett. **95**, 146802 (2005).